Adsorption 4, 225–231 (1998)

Evaluation of the Secondary Pore Structure of Hydrothermally- and Acid-treated Faujasite Type Zeolites

TAKAE KAWAI AND KAZUO TSUTSUMI
Toyohashi University of Technology, Tempaku-cho, Toyohashi 441-8580, Japan

Abstract. With regard to H-Y type zeolites dealuminated by hydrothermal and acid treatments, their physical properties were characterized by measurements of ^{29}Si- and ^{27}Al-MAS-NMR, IR, and X-ray diffraction. The secondary pores were quantitatively analyzed by the *t*-plot method for nitrogen adsorption isotherm at liquid nitrogen temperature and were then compared with the results of samples dealuminated by $SiCl_4$ treatment.

The plateau region of the nitrogen adsorption isotherm diminished as hydrothermal and acid treatments proceeded, with the result that the shape of the *t*-plot changed to that of three straight sections. This *t*-plot shape suggested that the secondary pores with relatively consistent sizes could develop with the progress of the treatment. On the other hand, $SiCl_4$ treatment was found to produce less secondary pores than hydrothermal and acid treatments. The surface area of micropores calculated from the *t*-plots gave a considerably higher value than values obtained from the BET equation and from that calculated geometrically. This is attributable to the micropore filling effect.

Keywords: faujasite, dealumination, hydrothermal treatment, acid treatment, secondary pore

1. Introduction

The framework of aluminosilicate type zeolites has aluminum atoms negatively charged, which are considered to be the origin of weak stability against thermal or acid treatment. Hence, a variety of dealuminating treatments have been reported and the acid and hydrothermal treatments or the combination of both are advantageous in that highly effective dealumination can be achieved by relatively simple procedures (Lynch et al., 1987; Maher et al., 1971; Scherzer, 1986). However, it is known (Horikoshi et al., 1989; Grobet et al., 1989) that these treatments partially destroy the zeolite framework, consequently generating secondary pores with wider distribution in the micro- or mesopore region in addition to the zeolitic primary pores regularly arrayed in the micropore region. The treatments also cause lattice defects such as the hydroxy nest at the site from which aluminum became detached (Grobet et al., 1989; Zukal et al., 1986).

In the present study structural analyses by means of ^{29}Si-, ^{27}Al-MAS-NMR, framework region IR, and X-ray diffraction were combined with the analysis of secondary pores by the *t*-plot method for faujasites which were dealuminated by hydrothermal and acid treatments. The results were also compared with those of faujasites dealuminated by $SiCl_4$ treatment (Kawai and Tsutsumi, 1992; Kawai et al., 1994).

2. Experimental

For original Na-$Y_{5.5}$ (Na_{51} $(AlO_2)_{51}$ $(SiO_2)_{141} \cdot nH_2O$) and hydrothermal- and acid-treated samples, those provided by Tosoh Corporation were used. Table 1 indicates the chemical composition of various samples. The $SiCl_4$ treatment, principally based on Beyer's technique (Beyer and Belenykaja, 1980), followed the method presented in our previous paper (Kawai et al., 1994), using Li, Na-$Y_{5.7}$ obtained by exchanging lithium ions with Na-$Y_{5.7}$ (Na_{50} $(AlO_2)_{50}$ $(SiO_2)_{142} \cdot nH_2O$) (Tosoh Corporation). The Si/Al ratio of $SiCl_4$-treated samples was calculated using the equation empirically obtained by Sohn et al. (1986) on the basis of the finding that

Table 1. Chemical compositions of the used samples determined by chemical analysis.

	SiO_2	Al_2O_3	Na_2O	SiO_2/Al_2O_3
	wt%			
Na-$Y_{5.5}$	67.1	20.6	12.5	5.5
H-Y_{14}	89.5	10.5	0.02	14.5
H-Y_{40}	95.6	4.0	0.03	40.4
H-Y_{144}	98.8	1.16	<0.05	144
H-Y_{770}	99.8	0.22	<0.01	770

These values were determined by Tosoh Corp.

the band shift of the symmetric stretching of O-T-O (T = Si or Al) given by the IR spectrum of the framework vibration region was linearly related to the ratio.

The ^{29}Si- and ^{27}Al-MAS-NMR were measured with JEOL JNM-EX270. The standard of ^{29}Si was set such that the polydimethylsilane peak occurred at −34.0 ppm. That of ^{27}Al was set such that the aluminum sulfate was 0 ppm. X-ray diffraction was measured using Philips PW1729 diffractometer. The IR spectrum was measured by the KBr wafer method using infrared spectrometer JASCO IR-810. Sample wafers were prepared by fully mixing KBr and samples at the weight ratio of 300 : 1 and pressing the resulting mixture in a vacuum onto dies 13 cm in diameter, with a pressure of 29 MPa. The wave number was corrected with a polystyrene film.

Nitrogen adsorption was measured with conventional automatic volumetric adsorption apparatus. Approximately 200 mg of the sample was taken into a sample vial, and then pretreated by heating at 673 K under vacuum of 1 mPa for 5 h. The adsorption was measured at liquid nitrogen temperature.

3. Results and Discussion

Figure 1 represents the results of ^{29}Si-MAS-NMR measurement of the samples. Original Na-$Y_{5.5}$ has four peaks corresponding to Si(0Al), Si(1Al), Si(2Al), and Si(3Al). The spectrum was deconvoluted for the digital curve and the Si/Al ratio in the framework was calculated from the area ratios of all peaks. The value thus obtained was 2.71, which agreed well with 2.76, the Si/Al ratio calculated from the results of chemical analysis shown in Table 1. In the spectra of samples H-Y_{14} through H-Y_{770} dealuminated by hydrothermal and acid treatments, only one peak attributed to Si(0Al) was noted, indicating that the framework scarcely

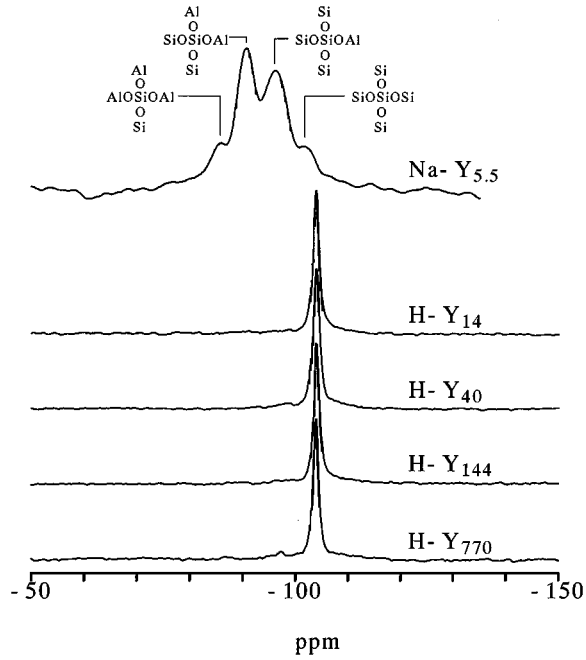

Figure 1. ^{29}Si-NMR spectra of original and treated samples.

included aluminum atom, which demonstrates that the hydrothermal and acid treatments achieved a high ratio of dealumination. Figure 2 shows the results of ^{27}Al-MAS-NMR measurement. Whereas Na-$Y_{5.5}$ had only one peak of tetrahedrally coordinated species

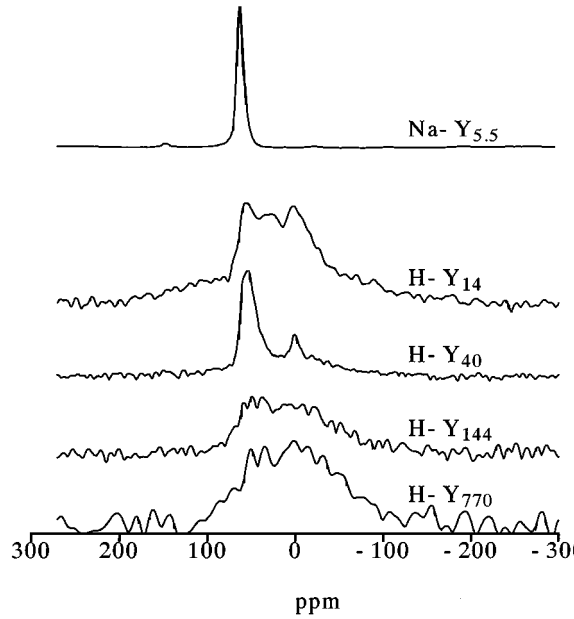

Figure 2. ^{27}Al-NMR spectra of original and treated samples.

Table 2. Extra-framework aluminum species (Scherzer, 1986).

Neutral	Cationic
Al_2O_3	Al^{3+}
$Al(OH)_3$	AlO^+
AlO(OH)	$Al(OH)^{2+}$
	$Al(OH)_2^+$

assigned to aluminum in the framework at about 50 ppm, treated samples showed another peak, octahedrally coordinated, assigned to the extra-framework aluminum species (Table 2 (Scherzer, 1986)), in the vicinity of 0 ppm. In contrast to the high proportion of extra-framework aluminum in H-Y_{14}, the proportion in H-Y_{40} was noticeably low. In hydrothermal treatment it is generally accepted that detached aluminum remains in the zeolite pores as an extra-framework aluminum species. It is also accepted that the subsequent dealumination of hydrothermally treated zeolite by acid treatment causes the extra-framework aluminum species as well as partial intra-framework aluminum to elute and to be removed. This indicates that the results described above correspond to the dealumination of H-Y_{14} solely by the hydrothermal treatment and the dealumination of H-Y_{40}, H-Y_{144} and H-Y_{770} by the combination of hydrothermal and acid treatments. Since the aluminum content in H-Y_{144} and H-Y_{770} is limited, the S/N ratio turns out to be high to give rise to a clear peak, whereas the spectral shape is close to that of H-Y_{14}, which implies the existence of both intra and extra-framework aluminum species.

Figure 3 shows the IR spectra of various samples in the framework vibration region. The spectra indicate that the treatments caused the absorption bands of the O-T-O (T = Si or Al) asymmetric stretching (in the vicinity of 1014 cm^{-1}) and of the symmetric stretching (in the vicinity of 784 cm^{-1}) to shift toward the higher wave numbers. This result suggests that aluminum atoms are removed from the framework. In all treated samples, the magnitude of shift was virtually the same, indicating that the extent of acid treatment does not affect the shift of the IR band in the framework vibration region. Sohn et al. (1986) deduced an equation representing the relationship between the amount of intra-framework aluminum and the magnitude of shift of the IR band in the framework vibration region for Na-type faujasites. The calculation of the amount of intra-framework aluminum, applying the equation to hydrothermal-treated H-Y_{14}, gives 3 Al per unit

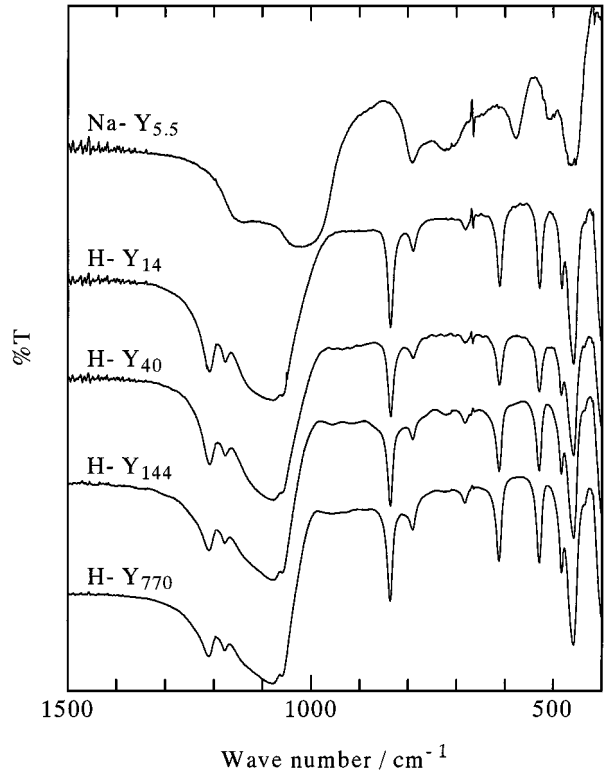

Figure 3. IR spectra of original and treated samples.

cell, a value considerably smaller than that obtained from chemical analysis. The aluminum amount in the chemical analysis should include both the amounts of the intra- and extra-framework aluminum. These results accompanied with those of the ^{27}Al-NMR measurement mentioned above demonstrate that the extra-framework aluminum species exist in a greater amount in H-Y_{14} than does the intra-framework aluminum. It can be said therefore, that the value given by the IR band shift was acceptable as the intra-framework aluminum.

Figure 4 represents the X-ray diffraction diagrams of various samples. Compared with original Na-$Y_{5.5}$, all treated samples showed that the peak position shifted toward the higher angle side. A decrease in the lattice constant shown in Table 3 suggests that the intra-framework aluminum is removed. In all treated samples the magnitude of shift is consistent and the lattice constant remains virtually the same; these tendencies are similar to the results of the IR spectral measurement in the framework region mentioned earlier, leading to the same conclusion that the extent of acid treatment does not affect the lattice constant. The integral intensities of X-ray diffractograms did not change so much,

Table 3. Lattice constant, crystallite size, Si/Al and number of aluminum atoms per unit cell.

	Lattice constant (nm)	Crystallite size (nm)	Si/Al_{IR}	Si/Al_{XRD}	N_{Al}/UC_{IR}
Na-$Y_{5.5}$	2.476	49	2.4	3.1	56
H-Y_{14}	2.427	36	61	110	3.1
H-Y_{40}	2.428	38	40	67	4.7
H-Y_{144}	2.429	39	34	110	5.5
H-Y_{770}	2.426	36	84	240	2.3

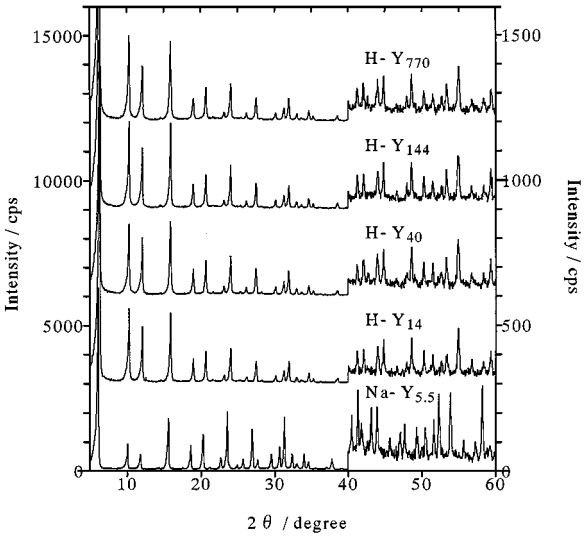

Figure 4. X-ray diffraction patterns of original and treated samples.

indicating that the crystallinity essentially remained after the treatments. However, a decrease in the crystallite size of treated samples (Table 3) suggests that the treatments partially destroyed the zeolite crystal lattice.

Figure 5 represents the adsorption isotherms of nitrogen at liquid nitrogen temperature. In the isotherm of untreated Na-$Y_{5.5}$ a distinctive plateau region exists, showing the shape of type I in the BDDT classification (Brunauer et al., 1940), which indicates that the pore size is sharply distributed. However, as the Si/Al ratio increases, i.e., as hydrothermal and acid treatments proceed, the plateau region disappears, the isotherm shape becoming closer to that of type II. This result suggests that hydrothermal and acid treatments develop secondary pores with wider pore size distribution. In H-Y_{14} the amount of adsorption decreased more than in other samples. This decrease, as indicated by the results of ^{27}Al-NMR measurement presented earlier, is considered attributable to partial blocking of zeolite pores

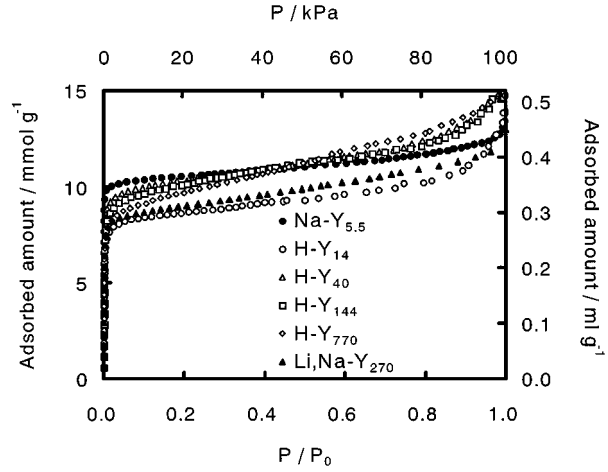

Figure 5. Adsorption isotherms of nitrogen at liquid nitrogen temperature on original and treated samples.

caused by detached aluminum remaining in the pores as a result of hydrothermal treatment. In H-Y_{40} through H-Y_{770} the amount of adsorption increased as a result of the elution of the remaining aluminum caused by acid treatment. These results coincided with the findings obtained from the IR spectra and X-ray diffraction in the framework vibration region.

The adsorbed amount on Li, Na-Y_{270} of $SiCl_4$-treated samples slightly decreased, which is considered attributable to partial destruction of the zeolite framework caused by the treatment or to the blocking of pores by the $Na(AlCl_4)$ complex, a by-product of $SiCl_4$ treatment (Kawai et al., 1994). The magnified view of the low-pressure side of Fig. 5 is shown in Fig. 6. In

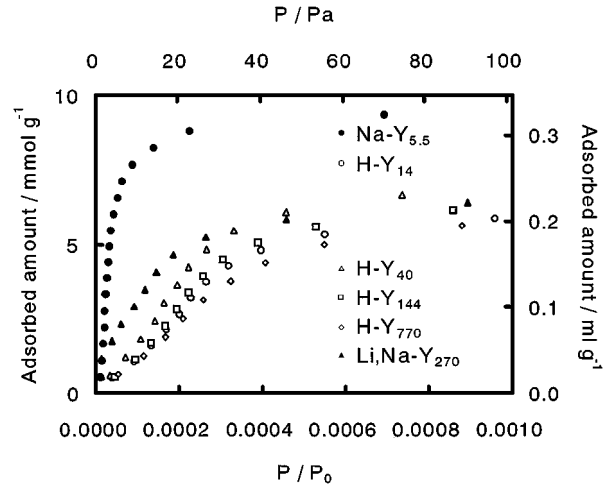

Figure 6. The magnified view of the low-pressure side of Fig. 5.

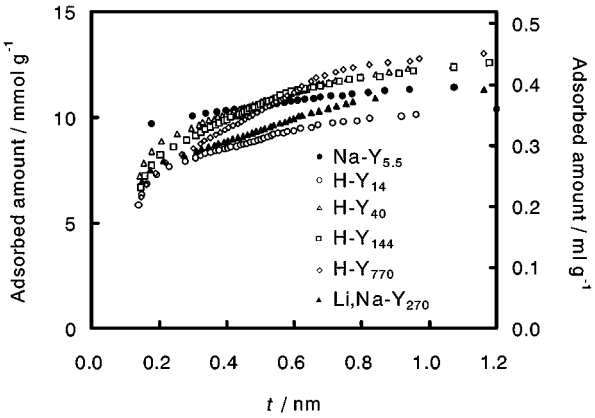

Figure 7. The t-plot curves of nitrogen adsorption.

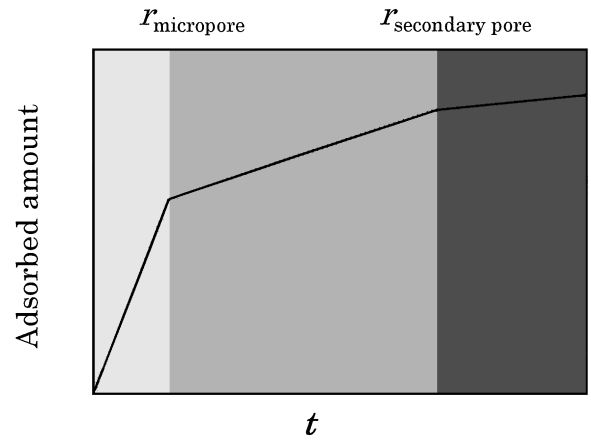

Figure 8. The adsorption growth scheme in t-plots consisting of three straight lines.

Na-$Y_{5.5}$ the isotherm rapidly rises at extremely low pressure, suggesting that Na-$Y_{5.5}$ and nitrogen molecules interact rather strongly each other. Na-$Y_{5.5}$ has great amount of aluminum atom in the framework, thus producing a strong electrostatic field. The above result is thus considered to be due to the interaction between the electrostatic field gradient on the Na-$Y_{5.5}$ pore surface and the quadrupole of nitrogen molecules, in addition to the presence of the regular pore structure of molecular dimension. The other noticeable point is that the initial rise in the Li, Na-Y_{270} of the $SiCl_4$-treated samples was more enhanced than those in hydrothermal and acid-treated samples, indicating that $SiCl_4$ treatment is more advantageous in terms of the retaining the regular pore structure.

Figure 7 represents the t-plot curves of nitrogen adsorption on the original and treated samples that were obtained from nitrogen adsorption isotherm of nonporous silica, Aerosil, at 77 K as the master curve. The t-plot of original Na-$Y_{5.5}$ gives a straight line without any inflexion. Since the lower limit of the master t-curve on the low pressure side is 0.14 nm, it was impossible to calculate data below the limit. Thus an inflexion of Na-$Y_{5.5}$ may appear below the lower limit, which permits, the inference that the calculated micropore radius would be smaller in Na-$Y_{5.5}$ than in other samples and the micropore surface area be greater. In treated samples, on the other hand, the t-plots consist of three straight lines, and this tendency becomes more distinctive as the treatment becomes more intensive.

Figure 8 illustrates the adsorption growth scheme in t-plots consisting of three straight lines. In the initial stage of adsorption, adsorption proceeds in all surfaces including micro- and mesopore surfaces as well as crystal external surface. Thus, the slope of t-plots in the initial stage of adsorption gives the total surface area. When t becomes equal to the micropore radius as adsorption proceeds, the zeolitic micropores are filled with the adsorbate, changing the adsorption site to the secondary pore surface, that is wider micropore or mesopore surface, and external surface with the result of the appearance of an inflexion in the t-plots. The value of t at the inflexion gives the micropore radius. The slope of the t-plots following this inflexion gives the surface area of surfaces other than the micropore surface, i.e., the secondary pore and external surfaces. The ordinate intercept of this straight line gives the micropore volume. When t is equal to the secondary pore radius, as adsorption further proceeds, the secondary pores are filled, giving rise to the second inflexion in the t-plots. The t value at this inflexion gives the secondary pore radius. Finally, adsorption is limited to the zeolite crystal external surface. The slope of the final part of the t-plots gives the area of the crystal external surface, and the ordinate intercept of this straight line gives the sum of the zeolitic micropore and secondary pore volumes. If secondary pore sizes are widely distributed, the pores are filled gradually as t grows larger, consequently forming a curve not a straight line. However, the fact that distinctive straight lines occur in hydrothermal and acid-treated samples suggests that the secondary pore sizes resulting from the treatments are rather consistent.

In hydrothermal and acid-treated samples, the first inflexion appears in the vicinity of $t = 0.2$ nm and the second in the vicinity of $t = 0.7$ nm. The t value at the first inflexion was smaller than 0.38 nm; the radius of the faujasite entrance. It is plausible that this

Table 4. BET surface area and respective surface areas calculated from *t*-plot.

	S_{BET}	All	Micro	Secondary	External
	$m^2\ g^{-1}$				
Na-$Y_{5.5}$	667	(12300)	(12200)	49	27
H-Y_{14}	551	1500	1340	125	33
H-Y_{40}	646	1770	1590	130	42
H-Y_{144}	658	1620	1380	185	57
H-Y_{770}	637	1470	1170	250	51
Li, Na-Y_{270}	601	1630	1450	134	43

measurement turned out to give smaller value than the real because of the micropore filling effect described later. The value at the second inflexion indicates that the secondary pore radius is ca. 0.7 nm. In such pores, the micropore filling has no significant effect and this radius is close to reported values ranging from 0.8 to 2.0 nm (Lohse et al., 1980; Lohse and Mildebrath, 1981). The existence of the straight section in the middle suggests that hydrothermal and acid treatments develop the secondary pores rather consistent in size. The total surface area calculated from the slope of the first straight section in the *t*-plots, the sum of the secondary pore surface area and the external surface area from the subsequent straight section, the external surface area from the next subsequent straight section, and the respective surface areas calculated from the values thus obtained are shown in Table 4 with the surface area calculated by the BET method. The total surface area and the micropore surface area calculated from *t*-plots gave greater values than the surface area calculated using the BET method. The geometric calculation of the surface area of Y-type zeolite based on its structural data gave approximately 700 m^2/g-dry, agreeing well with the result of the calculated value by the BET method. This suggested that the BET method, although being considered inadequate to microporous materials, could give reasonable value, whereas that the total surface area and micropore surface area calculated from *t*-plots would be unreasonable. The *t*-plot method requires the conditions that the BET constant *C* of the sample be close to that of the reference solid for the master *t*-curve and also that the pores consist of meso- or macropores. In the presnt study, the nitrogen adsorption isotherm for nonporous silica whose chemical composition is similar to that of zeolite was used as the master *t*-curve. Even if the chemical composition is similar, however, adsorbate molecules receive only unilateral effects from the silica surface. On adsorbents with channel-type micropores such as zeolites, the adsorbate molecules are subject to interact with the whole circumference (micropore filling effect). It is possible that the reason why the micropore surface area in zeolite determined from *t*-plots gives an abnormally high value is that the micropore filling effect increases the value of *t* in zeolite pores over the level in nonporous silica at the same pressure. In Na-$Y_{5.5}$ it is probable that the interaction between the strong surface electrostatic field gradient and the quadrupole of nitrogen molecules, in addition to the pore filling effect, still increased *t* value.

The micropore filling effect is greater enhanced, the smaller the pore size is. Conversely the greater the pores, the less significant the filling effect. Therefore, when nitrogen molecules adsorb on the zeolitic primary pores, the pore filling gives a great effect, whereas the effect is limited when adsorbed in the secondary pores. These findings support the conception that the secondary pore surface and the crystal external surface areas calculated from the slope of the straight line in the middle and last section of *t*-plots are relatively reliable. In hydrothermal and acid-treated samples, as the treatments proceed, the micropore surface area decreases (excluding H-Y_{14}) whereas the secondary pore surface area increases. This result coincides with the knowledge that hydrothermal and acid treatments develop secondary pores. The external surface area increases as well, which corresponds to the decreased crystallite size obtained from the results of X-ray diffraction measurement mentioned earlier. Table 5 represents the results of the micropore and secondary pore volumes calculated from the ordinate intercepts of the straight lines of the *t*-plots. Being calculated from the slopes of the straight line in the middle section, these values are considered relatively free from

Table 5. The micropore and mesopore volumes calculated from *t*-plots.

	All	Micro	Secondary
	$ml\ g^{-1}$		
Na-$Y_{5.5}$	0.368	0.328	0.040
H-Y_{14}	0.320	0.233	0.087
H-Y_{40}	0.387	0.285	0.102
H-Y_{144}	0.370	0.247	0.123
H-Y_{770}	0.392	0.207	0.185
Li, Na-Y_{270}	0.342	0.237	0.105

the effect of micropore filling and therefore more reliable. With the progress of the treatment, the micropore volume decreases whereas the secondary pore volume increases (excluding H-Y_{14}).

In $SiCl_4$-treated sample as well, the three straight sections were identified, suggesting the presence of the secondary pores. Despite of its higher Si/Al ratio, however, the secondary pore surface area in Table 4 and the secondary pore volume in Table 5 are rather small. These results indicate that the $SiCl_4$ treatment is more advantageous from a viewpoint that the development of the secondary pores can be inhibited.

4. Conclusion

Extra-framework aluminum species were identified by means of various characterizations of H-Y series dealuminated by hydrothermal and acid treatments, revealing that the extent of acid treatment does not affect the IR band shift or lattice constant. With the progress of hydrothermal and acid treatments, the shape of adsorption isotherm changes, producing distinct changes also in *t*-plots. The profile of *t*-plots indicated that hydrothermal and acid treatments developed the secondary pores in relatively consistent size around 0.7 nm in radius. It was proven possible to apply the *t*-plot method to the quantitative analyses of the secondary pore surface and the external surface areas as well as micropore and secondary pore volumes. However, the micropore surface area gave a considerably greater value because of the micropore filling effect.

Acknowledgment

The authors are grateful to Mr. S. Asano of Tosoh Corporation for his kind supply of zeolites.

References

Beyer, Hermann K. and I. Belenykaja, "A New Method for the Dealumination of Faujasite-type Zeolites," *Catalysis by Zeolites*, B. Imelik et al. (Eds.), p. 203, Elsevier, Amsterdam, 1980.

Brunauer, S., L.S., W.E. Deming, and E. Teller, "On a Theory of the van der Waals Adsorption of Gases," *J. Amer. Chem. Soc.*, **62**, 1723–1732 (1940).

Grobet, P.J., H. Geerts, M. Tielen, J.A. Martens, and P.A. Jacobs, "Framework and Non-Framework Al Species in Dealuminated Zeolite Y," *Stud. in Surface Sci. and Catal.*, **46**, 721–734 (1989).

Horikoshi, H., S. Kasahara, T. Fukushima, K. Itabashi, T. Okada, O. Terasaki, and D. Watanabe, "Study of Mesopores Induced by Dealumination in Zeolite Y," *Nippon Kagaku Kaishi*, 398–404 (1989).

Kawai, T. and K. Tsutsumi, "Evaluation of Hydrophilic-Hydrophobic Character of Zeolites by Measurements of their Immersional Heats in Water," *Colloid and Polymer Science*, **270**, 711–715 (1992).

Kawai, T., T. Yanagihara, and K. Tsutsumi, "Adsorption Characteristics of Chloroform on Modified Zeolites from Gaseous Phase as well as its Aqueous Solution," *Colloid and Polymer Science*, **272**, 1620–1626 (1994).

Lohse, U. and M. Mildebrath, "Dealuminated Y-type Molecular Sieves. Porosity of Dealuminated Molecular Sieves," *Z. Anorg. Allg. Chem.*, **476**, 126–135 (1981).

Lohse, U., H. Stach, H. Thamm, W. Schirmer, A. Isirikjan, N. Regent, and M. Dubinin, "Dealuminated Molecular Sieves of Y type. Determination of Micro and Secondary Pore Volumes by adsorption measurements," *Z. Anorg. Allg. Chem.*, **460**, 179–190 (1980).

Lynch, J., F. Raatz, and P. Dufresne, "Characterization of the Textural Properties of Dealuminated HY Forms," *Zeolites*, **7**, 333–340 (1987).

Maher, P.K., F.D. Hunter, and J. Scherzer, "Crystal Structures of Ultrastable Faujasites," *Adv. Chem. Ser.*, **101**, 266–278 (1971).

Scherzer, J., "The Preparation and Characterization of Aluminum-Deficient Zeolites," *ACS Symp. Ser.*, **248**, 157–200 (1986).

Sohn, Jong R., S.J. DeCanio, and Jack H. Lunsford, "Determination of Framework Aluminium Content in Dealuminated Y-type Zeolites: A Comparison Based on Unit Cell Size and Wavenumber of I.R. Bands," *Zeolites*, **6**, 225–227 (1986).

Zukal, A., V. Patzelova, and U. Lohse, "Secondary Porous Structure of Dealuminated Y Zeolites," *Zeolites*, **6**, 133–136 (1986).